Proceedings of the ASME 2015 34th International Conference on Ocean, Offshore and Arctic Engineering
OMAE2015
May 31-June 5, 2015, St. John's, Newfoundland, Canada

OMAE2015-41348

LOAD UNCERTAINTIES EFFECTS ON THE FATIGUE LIFE EVALUATION BY THE COMMON STRUCTURAL RULES

Po-Kai Liao **Yann Quéméner** **Chi-Fang Lee** **Kuan-Chen Chen**

Research Department
CR Classification Society
Kobe, Japan

ABSTRACT

This study evaluated the fatigue life of various hot spots located amidship a handy size oil tanker and a capesize bulk carrier. Specifically, the fatigue was evaluated accordingly to the harmonized common structural rules for bulk carriers and oil tankers recently released by the international association of classification societies. This study examined the stillwater and wave loads uncertainties effect on the fatigue life assessment. Hydro-structure coupling analyses were thus carried out enabling direct hydrodynamic load computations and accurate structural response assessment by finite element analyses. The comparison between direct and rules assessment allowed to identify the load uncertainties effect on the fatigue evaluation. As a result, the fatigue life evaluated by both approaches was significantly different, as expected with regard to the stillwater and dominant wave loads deviations. In addition, the study showed that the influence of the subjected loads was underestimated by the rules, leading to overestimated hot spot stress.

Keywords: wave load, potential flow, fatigue, harmonized common structural rules (CSR-H)

1. INTRODUCTION

Fatigue cracking due to cyclic loading is a common mode of damage in ship structure that can be mitigated by proper fabrication procedure and structural design. The IACS is presently on the final stage of development of the harmonized common structural rules (CSR-H) for bulk carriers and oil tankers [1] that include a fatigue evaluation procedure to verify that the fatigue life of any critical structural detail is at least greater than 25 years. This criterion complies with the newly adopted goal based ship construction standards (GBS) [2] resolution of the IMO.

The GBS requires also to provide the "explanation of the effect of uncertainties/assumptions on fatigue life, highlighting any margins used in fatigue calculations". The IACS has thus released a technical background report [3] that presents a sensitivity analysis for the fatigue evaluation. The report concluded that no margin is explicitly taken, but for the design S-N curves that corresponds to 97.7% of survival probability. The rules are also established in such a manner that the "effect on the fatigue damage due to uncertainty in the load and load effects is usually comparable or greater than effects from the uncertainty in the capacity". The hot spot stress calculation method and S-N curve measurements was developed jointly as addressed by Maddox [4], Fricke [5], Lotsberg [6] and [7], and as such the effects of their respective uncertainties should be inherently balanced, although Parunov et al [8] showed for stress concentration factor of longitudinal stiffeners end connections that the finite element methods using shell elements generated conservative results.

On the contrary, some assumptions are extremely conservative like the North Atlantic wave environment considered all along the ship life. The IACS [9] showed that most of ships do not operate permanently in such a stringent environment. However, under this assumption, the fatigue life predictions are deemed to have sufficient safety margin against the effect of whipping and springing that are not explicitly considered in the rules, but for which advanced analysis methods have been developed recently as reviewed by Hirdaris et al [10].

The sensitivity of the long term prediction of loads to the assumed operational conditions has also been investigated by various researchers. Soares and Moan [11] have analyzed the influence of the ship speed and wave environment on the fatigue loads assessment. Gregersen et al [12] have shown the high sensitivity of fatigue loads predictions to the 104 wave environment areas defined by the BMT [13] in their Global Wave Statistic (GWS). Gregersen et al [14] have also contributed to establish the North Atlantic wave environment scatter diagram and associated Pierson-Moskowitz wave spectrum that is presently recommended by the IACS [15] for the evaluation of unrestricted ship operation loads.

Afterwards, for the fatigue assessment, the load distribution over the ship life needs to be defined. Soares and Moan [11] and later Gregersen et al [12] have fitted a two-parameter Weibull distribution scaled on the extreme load value at $P=10^{-8}$ and showed that the shape parameter varied strongly with the ship length, but also with the considered wave environment. Recently, the rules have adopted a more simple approach that consists in scaling a two-parameter Weibull distribution on loads at a 10^{-2} probability level which, based on the typical S-N curve shape, corresponds to the stress level contributing the most to the accumulated fatigue damage. The shape factor is then set to unity to minimize the fitting error as demonstrated by Derbanne et al [16].

Finally, the rules loads have been formulated by regression conducted on direct hydrodynamic load evaluations through strip theory method computations. The IACS [17] reported that the loads evaluated by strip theory are generally on the conservative side. In the past, Parunov et al [18] already observed that the strip theory method leads to large overestimates of vertical wave bending moment amidship compare to the IACS [19] design loads. Therefore, for the rules development more advanced three dimensional potential flow theories were employed to validate the design values, and eventually full-scale measurements were also employed to verify both computational approaches. The question of the accuracy of computational method without full-scale measurement validation was already raised by Quéméner et al in a previous study [20] that produced significantly larger load evaluations compare to the rules values whereas the computational approach was similar to the three dimensional Green function method employed by the IACS [17].

Therefore, this study compared the fatigue evaluated by the rules and by advanced hydro-structure coupled analyses under the rules assumptions of unrestricted operation profile. The comparison of both results can highlight the effect of load uncertainties on the fatigue evaluation. Specifically, this study examined the fatigue life of various hot spots located amidship in a handy size oil tanker and a capesize bulk carrier.

This study consists of four sections. The first section presents the fatigue evaluation procedures by the rules and by direct stress assessment through hydro-structure coupling analyses. The second section presents the hydro-structure modeling and includes direct assessment of the stillwater and wave loads. The third section evaluates the reference fatigue stress needed to compute the fatigue life. Finally, the fourth section discusses on the fatigue results derived from the reference fatigue stress range obtained by three different approaches.

2. FATIGUE ASSESSMENT APPROACHES

2.1 Rules fatigue assessment

This study evaluated the fatigue of various hot spot located amidship a handy size oil tanker and a capesize bulk carrier accordingly to the rules [1]. Figure 1 presents the flowchart of the rules fatigue assessment.

At first, for each representative loading condition and for each dominant load case given by the rules, the hot spot stress range is computed by finite element analysis (FEA). Afterwards, correction factors, including the mean stress effect, are employed to convert hot spot stress range into fatigue stress range. The rules dominant load cases have also been established though spectral analysis described in [17], so that the produced fatigue stress range are expected to be the long term value at a probability level $P = 10^{-2}$.

Then, the reference fatigue stress range ($\Delta\sigma_{FS}$) is determined as the maximum value over the 5 dominant fatigue load cases provided by the rules. The long term stress distribution is then represented by a two-parameter Weibull distribution for which the shape factor is set as unity and Eqn. (1) can compute the scale factor k.

$$k = \Delta\sigma_{FS} / \ln\left(10^2\right) \quad (1)$$

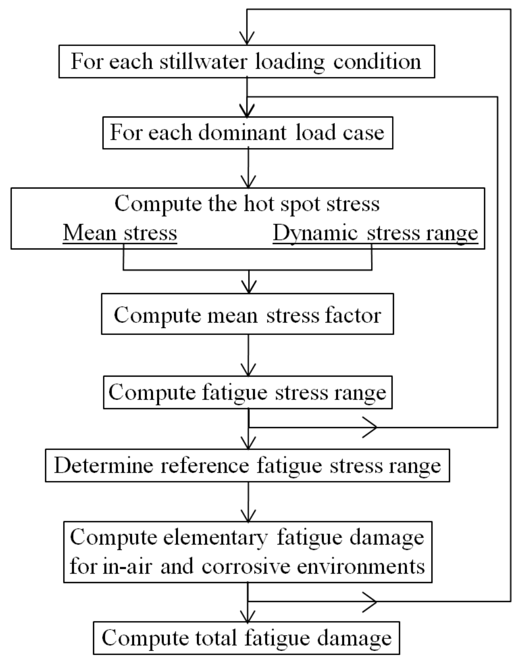

Figure 1: FLOWCHART OF THE RULES FATIGUE ASSESSMENT.

The elementary fatigue damages can thus be evaluated for each representative ship loading condition (see Table 1) and type of environment using the appropriate S-N curves as provided by the rules:

- in-air environment, for which the protection coating is effective, 80% of design life
- corrosive environment, 20% of design life.

Table 1: FRACTION OF LIFE TIME IN EACH LOADING CONDITION.

Loading condition	Oil tanker	Bulk carrier
Full load	50%	50%
Normal ballast	50%	20%
Heavy ballast	-	30%

Finally, the Miner's sum in Eqn. (2) can produce the total fatigue damage D_{tot} by combining the elementary damages weighted by their fraction of life time (α_i) in each loading condition and type of environment.

$$D_{tot} = \sum_i \alpha_i \cdot \left(80\% D_{Air,i} + 20\% D_{Corr,i}\right) \tag{2}$$

where $D_{air,i}$ and $D_{corr,i}$ are the elementary fatigue damage computed for in-air and corrosive environments' S-N curves respectively, and corresponding to the loading condition i.

This study evaluated the fatigue life accordingly to the rules using the software Veristar Hull edited by Bureau Veritas (BV)

2.2 Direct fatigue assessment

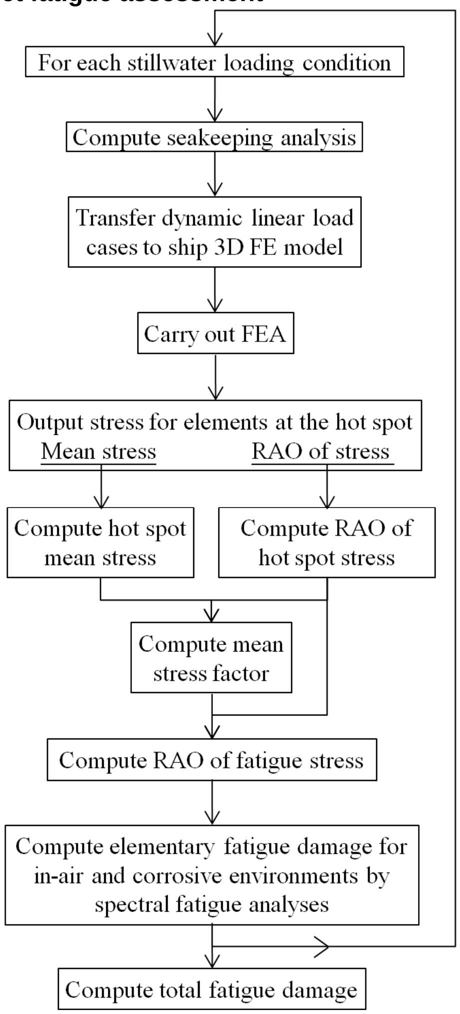

Figure 2: FLOWCHART OF THE DIRECT FATIGUE ASSESSMENT.

This study performed direct fatigue assessment through the hydro-structure coupling software Homer edited by Bureau Veritas (BV) that can transfer directly the dynamic linear loads computed by the hydrodynamic software Hydrostar (BV) to the 3D finite element model of the full ship. For each linear load case defined by a wave heading and frequency, the real and imaginary parts of the loads are transferred separately to the FE model. Afterwards, the ship static structural response is obtained by finite element analyses (FEA) that are carried out by NX Nastran. Finally, the RAO of fatigue stress can be extracted from the FEA results and the damage is evaluated by spectral fatigue analysis performed by StarSpec (BV). Figure 2 presents the flowchart of the direct fatigue assessment.

This method is much more complex to execute than the rules approach. However, whereas the rules concern is to provide a methodology that can be applied to any ship, the direct fatigue assessment has for advantage to allow for examining a given ship with more precision regarding:

- the stillwater loading conditions,
- the dynamic wave loads, and
- the structure response.

3. HYDRO-STRUCTURE MODELING

3.1 Hydrostatic balancing

This study performed hydro-structure computations on a handy size oil tanker and a capesize bulk carrier which the principal particulars are listed in table 2.

Table 2: SHIPS PRINCIPAL PARTICULARS.

	Oil tanker	Bulk carrier
Lpp (m)	174.0	226.2
B (m)	32.2	38
D (m)	17.3	20
T (m)	11.0	13.5
DWT (t)	40500	93300
V_s *(knt)*	14.6	15.7

For the direct fatigue assessment, the full ship FE model provides the mass properties. Figure 3 presents the ships FE models.

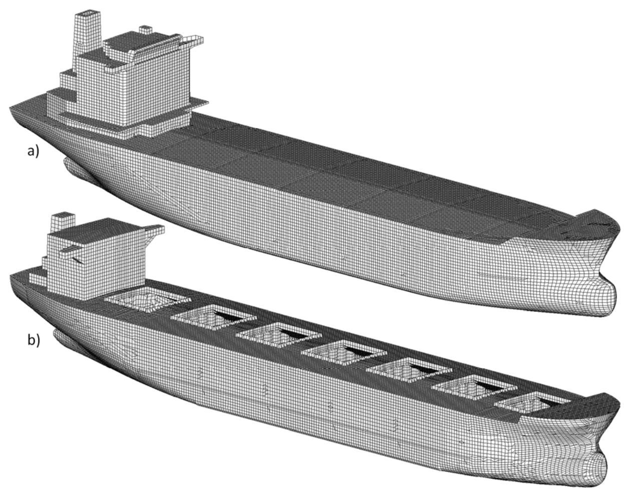

Figure 3: FE MODELS OF (a) THE OIL TANKER AND (b) THE BULK CARRIER.

At first, the FE model lightship weight and deadweight were calibrated to those provided by the loading manual. Additional mass elements were thus added to the structure to include the weight of equipment and cargo. Nastran RBE3 elements ensure an adequate load distribution from the mass elements to the related structural components, but it cannot reproduce the liquid pressure distribution. Therefore, for the tanks located amidship, where the fatigue was evaluated, the capacity solver of Homer was employed, so that the liquid pressure distribution can be reproduced accurately. The specific gravity and the mass of the cargo as well as the hydromesh of the tanks were thus provided. Figure 4 presents the hydromesh models of the immersed hull and the tanks located amidship.

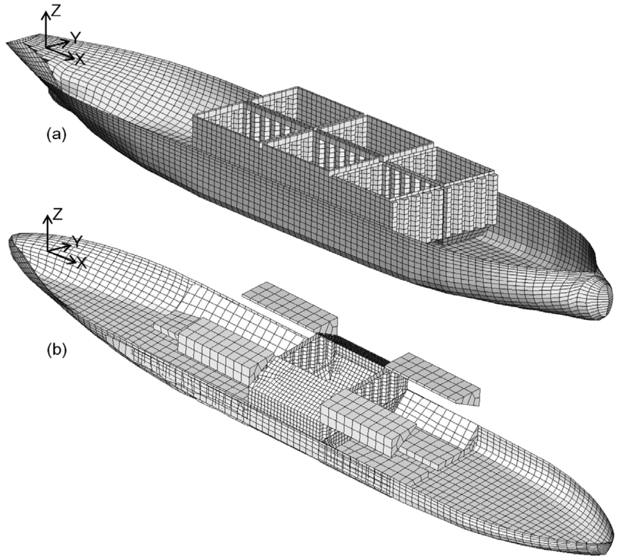

Figure 4: HULL AND TANKS HYDROMODELS FOR (a) THE OIL TANKER IN FULL LOAD CONDITION AND (b) THE BULK CARRIER IN HEAVY BALLAST CONDITION.

The hydromesh enables to integrate the pressure over the modeled geometry of the hull and the tanks. Only the wetted part of the hull and the tanks were modeled. Homer can then calculate the mass and the center of gravity of the tanks. Finally, combining the FE model mass and the tanks mass, the total weight of the ship and its center of gravity can be determined. Homer can also evaluate the hydrostatic properties of the immersed hull hydromesh. The hydromodel must be hydrostatically balanced before to run the seakeeping analysis. The offset vector between the hydromodel and the FE model coordinate systems must also be given to ensure the good transfer of loads between the two models.

Eventually, for each loading condition, the resulting stillwater bending moment distribution corresponded to that reported in the loading manual, whereas the rules stillwater bending moment for fatigue assessment was expressed as a fraction of the permissible values. Table 3 lists the stillwater bending moment considered for each loading condition and for each approach. Large deviations are observed between the two methods, especially for the ballast loading condition of each ship for which the rules value is approximately twice higher than that considered through the direct computations.

Table 3: STILLWATER BENDING MOMENT AMIDSHIP BY THE RULES AND DIRECT APPROACH.

Oil tanker, Stillwater bending moment (MN.m)			
Loading condition	Rules (1)	Direct (2)	(2)/(1)
Full	-519.2	-630.1	121%
Ballast	801.1	363.3	45%
Bulk carrier, Stillwater bending moment (MN.m)			
Loading condition	Rules (1)	Direct (2)	(2)/(1)
Full	-733.6	-661.9	90%
Normal ballast	1516.4	826.6	55%
Heavy ballast	-1375.5	-1451.6	106%

3.2 Wave loads direct computations

At first, seakeeping analyses are carried out using Hydrostar for a ship speed corresponding to 75% of the service speed as assumed by the rules [1]. The radiation and diffraction problems are thus solved to compute the pressures acting over the hull and in the tanks, and then to produce the ship hydrodynamic coefficients. Afterwards, the motion equations can be solved to evaluate the ship motions and accelerations.

Then, Homer can directly transfer the pressures on the structural mesh (i.e. FE model) as explained in [21]. This step is simply executed thanks to the source method employed by Hydrostar that provides a continuous representation of the potential through the wetted part of hull and tanks structural meshes. Homer can then recalculate the hydrodynamic coefficients by integrating the pressure over the hull structural mesh. Finally, the motion equations are solved with the new coefficients. In this study, the comparison of RAOs of motion showed a good agreement between Hydrostar and Homer computations that confirmed the correct loads transfer to the FE model. In addition, the FE model, when loaded, is inherently balanced as imposed by the motion equations solution.

After carrying out the seakeeping analyses, Homer can also extract the RAOs of the ship motions and the internal loads and sea pressure along the ship. The dominant wave loads were thus determined accordingly to the method described in [17]. Spectral analyses were carried out to determine amidship the load and accelerations long term value at a probability level of 10^{-2} for each of the dominant load case established in the rules and listed in Table 4. The spectral analyses were carried out based on the assumptions provided by the rules technical background [17]:

- North Atlantic wave scatter diagram
- Pierson-Moskowitz wave spectrum
- Angular spreading of the wave energy given by the function $\cos^2$
- Equal heading probability

Table 4: RULES DOMINANT LOAD CASES.

Abbreviation	Description
HSM	Maximum vertical bending moment amidships and maximum vertical acceleration at fore perpendicular in head sea
FSM	Maximum vertical bending moment amidships in following sea
BSR	Maximum roll motion in beam sea
BSP	Maximum pressure at waterline amidships in beam sea
OST	Maximum torsional moment in oblique sea

Tables 5 and 6 present the rules and direct load evaluations obtained for each dominant load case. The respective dominant loads correspond to the rules description provided in Table 4. However, for the oblique sea (OST) load case, the torsion moment was evaluated amidship instead of at the first and last quarter of the ship length, so that the load can be compared in way of the investigated hot spots.

It can be observed that for the head (HSM) and following (FSM) sea load cases, characterized by the wave vertical bending moment amidship (see Table 4), the direct computations predictions were approximately 30% higher than the rules values. Then, for the beam sea dominant load case (BSR), characterized by the roll acceleration at the center of gravity, the predictions were significantly larger than the rules especially for the ballast conditions of the bulk carrier for which the direct evaluations were twice greater than the rules values. Then, for the beam sea dominant load case (BSP), characterized by the wave pressure at the waterline amidship, the predictions were close to the rules. Finally, for the oblique sea dominant load case (OST), regarding the torsional moment taken amidship, the predictions deviated largely from the rules values; however this load is very low amidship and thus is not expected to be critical for the fatigue evaluation.

Table 5: OIL TANKER DOMINANT LOADS BY THE RULES AND BY SPECTRAL ANALYSIS.

Dominant load case	Load evaluation approach	Full	Normal ballast
HSM	Rules (1)	313.2	317.2
M_{wv}	Direct (2)	408.0	412.1
(MN.m)	(2)/(1)	132%	134%
FSM	Rules (1)	297.6	271.8
M_{wv}	Direct (2)	408.0	412.1
(MN.m)	(2)/(1)	139%	156%
BSR	Rules (1)	0.0189	0.0349
a_{roll}	Direct (2)	0.0224	0.0513
(rad.s^{-2})	(2)/(1)	119%	147%
BSP	Rules (1)	45.8	33.0
P_{ex}	Direct (2)	41.7	33.7
(kN/m^2)	(2)/(1)	91%	102%
OST	Rules (1)	26.4	25.5
M_{wt}	Direct (2)	26.0	38.1
(MN.m)	(2)/(1)	98%	149%

Table 6: BULK CARRIER DOMINANT LOADS BY THE RULES AND BY SPECTRAL ANALYSIS.

Dominant load case	Load evaluation approach	Full	Normal ballast	Heavy ballast
HSM	Rules (1)	680.0	692.0	690.5
M_{wv}	Direct (2)	888.5	777.5	972.0
(MN.m)	(2)/(1)	131%	112%	141%
FSM	Rules (1)	646.0	588.2	595.5
M_{wv}	Direct (2)	888.5	777.5	972.0
(MN.m)	(2)/(1)	138%	132%	163%
BSR	Rules (1)	0.0225	0.0274	0.0260
a_{roll}	Direct (2)	0.0336	0.0501	0.0502
(rad.s^{-2})	(2)/(1)	149%	183%	193%
BSP	Rules (1)	54.4	37.1	40.7
P_{ex}	Direct (2)	41.8	41.4	46.5
(kN/m^2)	(2)/(1)	77%	112%	114%
OST	Rules (1)	162.5	171.6	166.7
M_{wt}	Direct (2)	12.9	28.9	104.1
(MN.m)	(2)/(1)	8%	17%	62%

4. FATIGUE STRESS ASSESSMENT

4.1 Hot spot stress

In the local model, the hot spot areas were modeled accordingly to the very-fine-mesh rules requirements. The separate model extent was bounded by primary supporting structures. Close to the hot spot, the element size was set equal to the net thickness (t*t), but for the hatch corner which the free edge was divided in 15 elements accordingly to the rules. Figures 5 and 6 present the local FE models of the bulk carrier transverse bulkhead lower stool and hatch corner. The nodal displacements obtained from the global model FE analyses were then applied to the corresponding boundary nodes on the local model. The lateral pressures were also transferred from the load files of the global model. Finally, the FEAs were carried out and for the elements surrounding the hot spot, the RAOs of stress were extracted. Figures 7 and 8 present the examined hot spots marked "HS" and the corresponding structural details which the abbreviations definition are listed in Table 7.

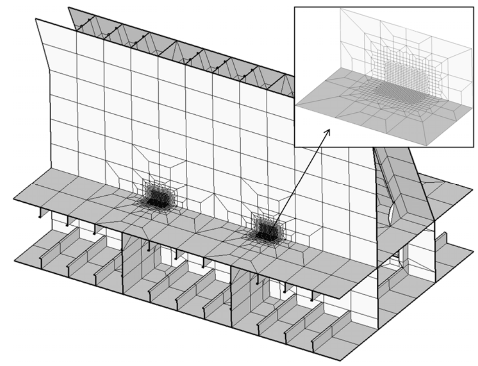

Figure 5: SEPARATE FE MODEL OF A TRANSVERSE BULKHEAD LOWER STOOL, VERY FINE MESH IN WAY OF THE LONGITUDINAL GIRDERS CONNECTIONS.

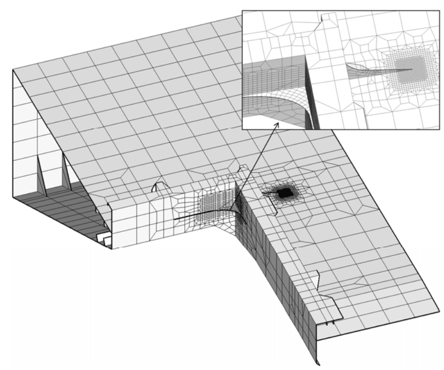

Figure 6: SEPARATE FE MODEL OF A HATCH COAMING, VERY FINE MESH IN WAY OF THE HATCH CORNER AND THE END BRACKET.

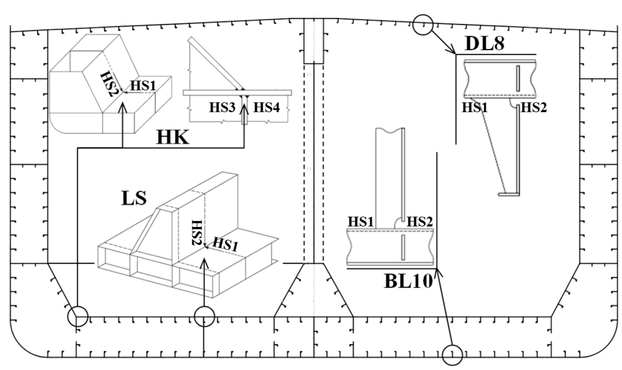

Figure 7: OIL TANKER MIDSHIP SECTION.

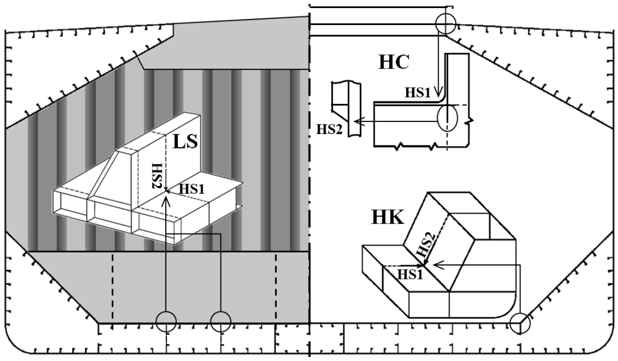

Figure 8: BULK CARRIER MIDSHIP SECTION.

Table 7: EXAMINED STRUCTURAL DETAILS.

Abbreviation	Description
DL8	Deck Longitudinal No.8 connection to deck transverse
BL10	Bottom Longitudinal No.10 connection to floor
HK	Hopper Knuckle connection to inner bottom
LS	Transverse bulkhead Lower Stool connection to inner bottom
HC	Hatch Coaming connection in way of the corner

The rules provide a complete procedure to convert the stresses extracted from the elements surrounding the hot spot into the fatigue stress needed to evaluate the fatigue through the design S-N curves. Figure 2 shows the steps that can produce the RAO of fatigue stress.

At first, the rules stress interpolation method can compute the mean stress and the RAO of stress both read out at the hot spot. The correction factor for mean stress effect can then be obtained as it relates to the mean stress and the long term value of hot spot stress range. Finally, the RAO of fatigue stress is derived from the RAO of hot spot stress and corrected by various factors including that regarding the mean stress effect as expressed in Eqn. (3).

$$\Delta\sigma_{FS} = f_{mean} \cdot f_{thick} \cdot f_c \cdot \Delta\sigma_{HS} \tag{3}$$

where f_{thick} is the correction factor for plate thickness, f_c is the correction factor related to the net scantling definition of the FE modeling (f_c=0.95), and f_{mean} is the factor for mean stress effect which the evolution is shown in Fig. 9.

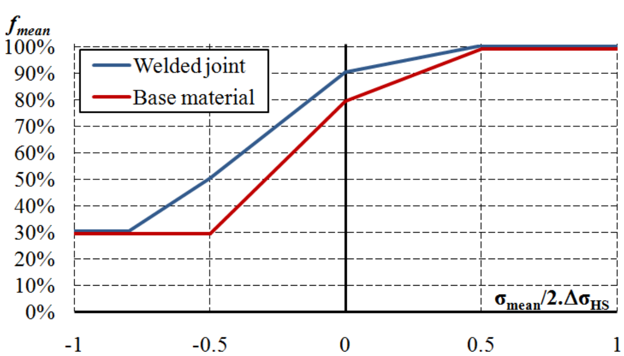

Figure 9: FACTOR FOR MEAN STRESS EFFECT.

4.2 Reference fatigue stress range evaluation by direct spectral analysis

The long term values of fatigue stress range at 10^{-2} probability level were directly evaluated by spectral analysis using the RAO of fatigue stress previously produced. The spectral analysis was carried out based on the rules assumptions [17] for design load assessment as presented in section 3.2. The obtained reference fatigue stress range can then be used to scale the two-parameter Weibull long term stress distribution as described in the rules (see section 1.1). The results are listed in the Tables 8 and 9 in the column marked "Direct".

4.3 Reference fatigue stress range evaluation by the Equivalent Design Wave method

This study employed the equivalent design wave (EDW) method to obtain the stress response that relates to the rules dominant loads. First, the peak value of the RAO of each dominant load was extracted with the corresponding wave frequency (ω_{max}) and phase angle (Φ_{EDW}). The EDW height was then calculated using Eqn. (4).

$$H_{EDW} = DL_{rules} / RAO_{DL-max} \tag{4}$$

where DL_{rules} is the dominant load rules value listed in Tables 5 and 6, and RAO_{DL-max} is the peak value of the RAO of dominant load produced by direct hydrodynamic analysis.

The hot spot stress response that relates to the considered dominant load EDW was then obtained using Eqn. (5) that expresses the linearity of the loads induced by the regular waves as assumed by the hydrodynamic computations.

$$\sigma_{HS}=RAO_{\sigma HS}\left(\omega_{max}\right)\cdot H_{EDW} \times cos\left(\Phi_{EDW}-\Phi_{\sigma HS}\left(\omega_{max}\right)\right) \tag{5}$$

where $RAO_{\sigma HS}(\omega_{max})$ is the RAO value of the hot spot stress taken at the EDW wave frequency ω_{max}, and $\Phi_{\sigma HS}(\omega_{max})$ is the phase angle of the hot spot stress taken at the frequency ω_{max}.

The obtained reference fatigue stress range can then be used to scale the 2-parameter Weibull long term stress distribution as described in the rules (see section 1.1). The results are listed in the Tables 8 and 9 in the column marked "EDW".

5. DISCUSSION OF THE RESULTS

5.1 Fatigue evaluation

This study has evaluated the fatigue damage and fatigue life using the rules approach that considers a two-parameter Weibull long term distribution of the fatigue stress range scaled on the reference fatigue stress range defined at a 10^{-2} probability level. Specifically, the reference fatigue stress range was obtained by three different methods:

- by the rules (see section 2.1),
- by spectral analysis (see section 4.2) performed using the RAO of fatigue stress obtained through direct stress assessment (see section 2.2), and
- by EDW approach (see section 4.3) performed using the RAO of fatigue stress obtained through direct stress assessment (see section 2.2).

Tables 8 and 9 list the detailed results of the fatigue life evaluations by the three approaches for the oil tanker and the bulk carrier respectively. Figures 9 and 10 present the fatigue life predictions by the three approaches for the hot spots presented in Figs. 7 and 8. It can be observed that for most of the hot spots, the fatigue life evaluated by the direct approach were significantly different from those obtained by the rules, as expected in view of the large deviations reported regarding the stillwater loads (see Table 3) and the dominant loads (see Tables 5 and 6) applied by each approach. By contrast, for some hot spots, it appears that the fatigue life predictions obtained through the EDW method were unexpectedly significantly larger than those produced by the rules, whereas the wave induced hot spot stress ranges were derived from the rules dominant loads. Therefore, three sources of load uncertainties to the fatigue life prediction are discussed in this section:

- the stillwater loads
- the wave dominant loads
- the wave subjected loads

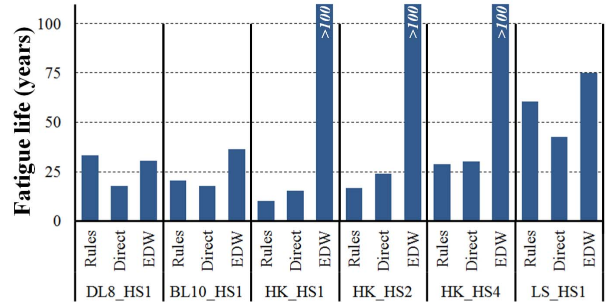

Figure 9: FATIGUE LIFE IN THE OIL TANKER.

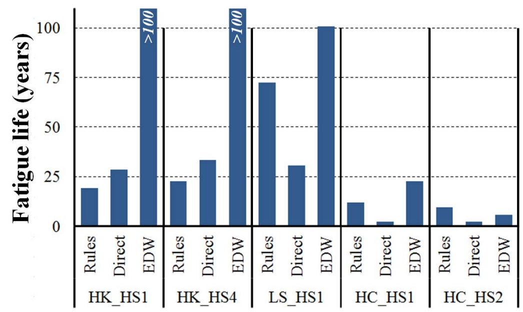

Figure 10: FATIGUE LIFE IN THE BULK CARRIER.

Table 8: FATIGUE LIFE EVALUATION BY THREE APPROACHES FOR VARIOUS HOT SPOTS IN THE OIL TANKER.

		DL8_HS1			**BL10_HS1**			**HK_HS1**			**HK_HS2**			**HK_HS4**			**LS_HS1**		
		Rules	Direct	EDW	Rules	Direct	EDW	Rules	Direct	EDW	Rules	Direct	EDW	Rules	Direct	EDW	Rules	Direct	EDW
Full	DLC	FSM	-	FSM	FSM	-	FSM	HSM	-	HSM	HSM	-	HSM	HSM	-	HSM	HSM	-	HSM
	$\Delta\sigma_{HS}$	66.4	106.2	76.8	70.7	59.4	54.3	125.0	112.4	25.6	107.7	91.2	31.0	80.1	83.0	21.3	58.4	65.3	51.9
	σ_{mean}	-35.1	-71.0	-71.0	-71.1	-90.5	-90.5	255.6	147.5	138.0	211.7	130.3	126.6	166.1	37.3	23.9	96.9	77.5	78.6
	f_{mean}	0.66	0.63	0.53	0.45	0.30	0.30	1.00	1.00	1.00	0.96	1.00	1.00	1.00	0.95	1.00	1.00	1.00	1.00
	$\Delta\sigma_{FS}$	41.9	63.8	38.7	30.2	16.9	15.5	118.7	105.8	24.4	102.4	86.9	29.5	76.9	74.3	18.3	55.4	61.9	49.9
Normal Ballast	DLC	HSM	-	HSM	HSM	-	HSM	BSP	-	BSP	BSP	-	BSP	BSP	-	BSP	HSM	-	HSM
	$\Delta\sigma_{HS}$	72.9	104.5	78.1	101.4	106.7	73.4	116.8	54.4	58.6	95.8	52.3	61.4	73.6	42.2	55.0	45.6	52.2	37.0
	σ_{mean}	84.9	50.2	50.2	86.1	121.1	121.1	-112	-44.7	-46.7	-108	-52.1	-59.4	-74.4	4.4	5.2	-51.0	-23.5	-23.5
	f_{mean}	1.00	0.95	0.96	1.00	1.00	1.00	0.42	0.55	0.58	0.39	0.50	0.51	0.50	0.91	0.91	0.40	0.72	0.65
	$\Delta\sigma_{FS}$	69.3	94.1	71.6	95.8	101.4	69.7	46.3	30.5	32.4	35.9	25.4	29.9	34.8	36.4	42.8	17.3	35.3	22.7
Fatigue	D_{tot}	0.60	1.78	0.63	1.50	1.77	0.52	3.03	2.05	0.05	1.88	1.09	0.05	0.77	0.71	0.10	0.24	0.39	0.17
	T_F	33.2	17.9	32.1	20.4	17.6	36.5	10.2	15.2	187.1	16.7	23.9	174.6	28.9	30.2	113.0	60.8	42.8	75.2

Table 9: FATIGUE LIFE EVALUATION BY THREE APPROACHES FOR VARIOUS HOT SPOTS IN THE BULK CARRIER.

		HK_HS1			**HK_HS4**			**LS_HS1**			**HC_HS1**			**HC_HS2**		
		Rules	Direct	EDW	Rules	Direct	EDW	Rules	Direct	EDW	Rules	Direct	EDW	Rules	Direct	EDW
Full	DLC	BSP	-	BSP	BSP	-	BSP	FSM	-	FSM	HSM	-	HSM	HSM	-	HSM
	$\Delta\sigma_{HS}$	134.6	79.5	24.1	106.8	64.3	28.6	39.5	38.1	26.1	159.4	281.3	183.2	123.2	223.9	174.5
	σ_{mean}	-36.8	-67.0	-76.0	-29.4	-17.2	-18.6	20.7	9.7	9.6	-65.4	-106	-106	-44.7	-97.4	-104
	f_{mean}	0.62	0.4	0.3	0.79	0.79	0.64	0.96	0.93	0.94	0.59	0.56	0.51	0.74	0.72	0.66
	$\Delta\sigma_{FS}$	79.7	36.7	6.9	80.2	48.4	15.7	34.0	42.4	29.5	92.2	154.1	91.1	86.3	154.2	109.7
Normal Ballast	DLC	BSP	-	BSP	BSP	-	BSP	HSM	-	HSM	HSM	-	HSM	HSM	-	HSM
	$\Delta\sigma_{HS}$	87.9	55.7	39.0	73.9	49.0	28.1	39.9	41.2	34.5	177.1	223.4	156.8	120.1	187.4	164.4
	σ_{mean}	-57.1	-39.1	-33.6	-55.0	-0.4	0.1	-60.4	-51.6	-52.2	160.3	74.8	74.8	100.4	108.1	104.6
	f_{mean}	0.37	0.38	0.56	0.60	0.90	0.90	0.30	0.40	0.30	0.98	0.87	0.51	0.99	0.96	0.96
	$\Delta\sigma_{FS}$	31.1	22.6	20.5	42.3	41.7	21.7	11.4	19.8	12.5	169.1	188.4	136.6	113.4	164.5	150.5
Heavy Ballast	DLC	HSM	-	HSM	HSM	-	HSM	HSM	-	HSM	HSM	-	HSM	HSM	-	HSM
	$\Delta\sigma_{HS}$	98.5	94.5	53.8	76.0	85.5	38.2	58.3	70.1	40.4	157.7	307.7	143.9	94.7	228.8	159.2
	σ_{mean}	366.9	253.5	261.6	343.1	265.5	266.5	234.4	197.9	199.0	13.6	-143	-143	-0.2	-125	-131
	f_{mean}	1.00	1.00	1.00	1.00	1.00	1.00	1.00	1.00	1.00	0.82	0.83	0.30	0.90	0.68	0.57
	$\Delta\sigma_{FS}$	93.6	89.7	51.2	72.2	75.5	31.6	55.4	84.7	48.8	125.3	248.7	42.4	106.1	138.3	86.2
Fatigue	D_{tot}	1.57	0.74	0.10	1.15	0.56	0.02	0.17	0.65	0.11	3.07	14.4	1.32	2.67	11.9	5.07
	T_F	20.1	29.7	117.0	23.3	34.5	339.7	75.3	31.8	105.2	12.1	2.3	22.6	11.8	2.5	6.1

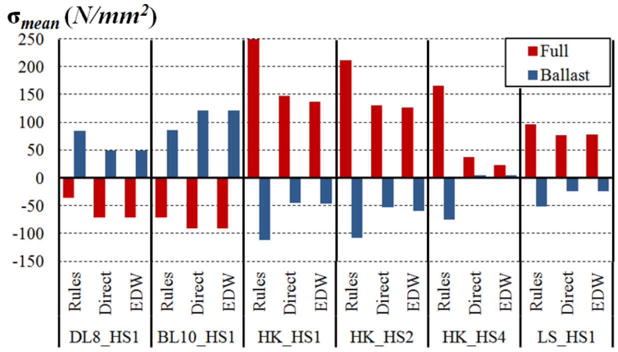

Figure 11: MEAN STRESS IN THE OIL TANKER.

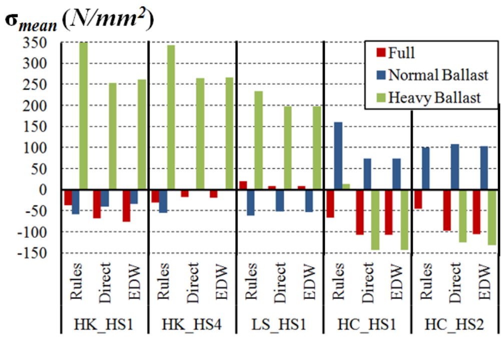

Figure 12: MEAN STRESS IN THE BULK CARRIER.

5.2 Stillwater loads effect

In section 3.1, significant deviations are observed between the rules stillwater bending moment and that of the real loading condition reported in the loading manual. Especially, in Table 3, it was observed that for the ballast conditions of both ships, the stillwater bending moments considered by the rules were approximately twice greater than the real value reproduced by the direct stress assessment approach. The stillwater load uncertainties can thus influence the hot spot mean stress evaluation and consequently the factor for mean stress effect (f_{mean}, see Fig. 9).

Figures 11 and 12 present the mean stress obtained for each loading condition and by the three stress approaches for the oil tanker and the bulk carrier respectively. It can be observed that the mean stress obtained by the direct stress assessments (see Figs. 11 and 12, "Direct" and "EDW") can largely deviate from the rules assessment. However, the mean stress does not directly affect the fatigue life because the factor for mean stress effect (f_{mean}) relates also to the wave-induced hot spot stress range as shown in Fig. 9. By contrast, the sign of the mean stress can have a significant influence on the factor for mean stress effect. Based on f_{mean} rules formulation, a tension mean stress can lead to a reduction of the hot spot stress until 20%, whereas a compressive mean stress can reduce the hot spot stress from 20% to 70%. The uncertainty of a compressive mean stress can thus have a larger effect on the fatigue life prediction than for a tension mean stress. For the oil tanker, in Fig. 9, it appears that every hot spot have a mean stress sign that alternates depending on the loading condition. According to the rules fraction of life time in each loading condition (see Table 1), the uncertainty in mean stress can thus only affect 50% of the total fatigue life contribution. Similar observations can be made for the bulk carrier.

5.3 Wave dominant loads effect

Section 3.2 compared the ship motions and internal loads direct evaluation to the rules values. In Tables 8 and 9, the rules assessment established that the critical dominant load cases amongst all the examined hot spots are the head (HSM), the following (FSM) and the beam (BSP) seas. In Tables 5 and 6, it can be observed that the direct evaluation of the wave pressures at the waterline amidship characterizing the BSP load case, were close to the rules value. By contrast, large deviations were observed regarding direct evaluations of the vertical bending moment for HSM and FSM that was approximately 30% higher than the rules values. The wave loads uncertainties can thus influence the hot spot stress range evaluation.

Figures 13 and 14 present the hot spot stress range evaluation by the three approaches for the oil tanker and the bulk carrier respectively. It can be observed that in the oil tanker at the examined deck longitudinal hot spot DL8_HS1, the hot spot stress range evaluated by the direct spectral analysis is higher than that obtained by the rules. In Table 8, it appears that the dominant load cases established during the rules assessment were the head sea (HSM) for the ballast condition and the following sea (FSM) for the full condition. Those load cases are characterized by the vertical wave bending moment for which the direct predictions (see Table 5) were approximately 30% higher than the rules. Therefore, the hot spot stress deviation observed in Fig. 13 between rules and direct assessments can be explained by the higher direct vertical bending moment evaluation. Similar observations can be made for the bulk carrier hot spots located on the hatch corner (i.e. HC_HS1 and HC_HS2, see Fig. 14).

In Figure 13 for the oil tanker, it appears then that at the examined bottom longitudinal hot spot BL10_HS1, the hot spot stress range evaluated by the direct spectral analysis is similar to that obtained by the rules. However, because the dominant load case obtained by the rules for both loading conditions were the head and the following sea (see Table 8; HSM and FSM), higher stress were thus expected as for DL8_HS1. The difference with the deck longitudinal lies on the fact that the bottom longitudinal was also subjected to sea and water ballast pressure. Those additional loads would thus reduce the vertical bending moment deviation effect on the hot spot stress. Similar observations can be made for the oil tanker's hopper knuckle in full condition and lower stool in both loading conditions, as well as for the bulk carrier's hopper knuckle in heavy ballast condition and lower stool in all loading condition, for which the dominant load cases were the HSM or FSM (see Tables 8 and 9), and were also subjected to water ballast and cargo oil pressure that would reduce the level of stress at those hot spots.

Finally, for the oil tanker, it can be observed that in ballast condition at the hopper knuckle hot spots (HK_HS1, HK_HS2 and HK_HS4), the dominant load case established during the rules assessment was the beam sea BSP (see Table 8). Although good agreements were found in Table 5 between sea pressure direct assessment and rules value, large hot spot stress reduction can be observed in Fig. 13. Here also, the subjected water ballast pressure would decrease the hot spot stress induced by the dominant load. Similar observations can be made for the bulk carrier hopper knuckle hot spots HK_HS1 and HK_HS4 for which the rules assessment established the beam sea BSP as dominant load case.

The comparison between direct spectral predictions and rules evaluations showed the influence of the load uncertainties identified in section 3.2 (see Tables 5 and 6) on the hot spot stress. The additional loads, also called by the rules "subjected loads" by opposition to the dominant loads, would thus have reduced the hot spot stress. The subjected load effect is explicitly analyzed in the next section.

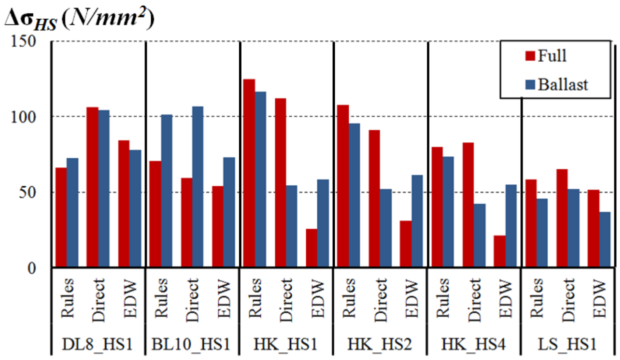

Figure 13: HOT SPOT STRESS RANGE IN THE OIL TANKER.

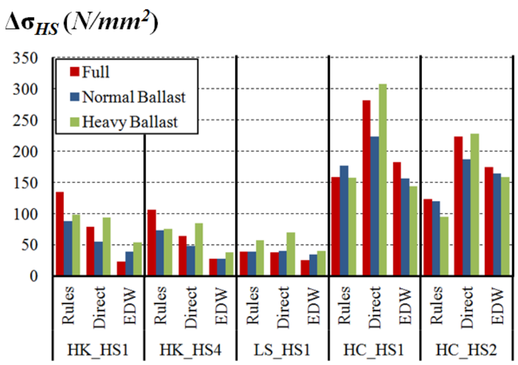

Figure 14: HOT SPOT STRESS RANGE IN THE BULK CARRIER.

5.4 Wave subjected loads effect

In section 5.3, it has been proposed that uncertainties in subjected loads evaluation could explain why the stress range obtained by direct spectral analysis were lower than expected based on the comparison of dominant loads evaluation by direct spectral analysis and by the rules. This study evaluated thus the stress response to the rules dominant loads using the stress RAO obtained by the direct stress assessment and employing the Equivalent Design Wave (EDW) methods. The stress range results are presented in Figs. 13 and 14 for the oil tanker and the bulk carrier respectively. The comparison of the wave induced hot spot stress produced by the rules and by the EDW method can then highlight the subjected load effect on the hot spot stress evaluation.

In Figures 13 and 14, considering hot spots located on deck (i.e. DL8_HS1 for the bulk carrier, and HC_HS1 and HC_HS2 for the bulk carrier) that are not subjected to additional loads, the level of stress range obtained by EDW method was similar to that calculated by the rules. Therefore, for those hot spots, the stress directly relates to the dominant load value, the vertical bending moment in this case.

Considering all remaining hot spots that are subjected to additional loads mainly induced by sea/ballast/cargo pressure, the level of stress range obtained by EDW method is significantly lower than that predicted by the rules. Therefore, the direct hydrodynamic computations led to higher predictions of the subjected loads than the rules. The subjected load uncertainties can thus have a significant effect on the hot spot stress evaluation.

6. CONCLUSION

This study has evaluated the fatigue of various hot spots located amidship a handy size oil tanker and a capesize bulk carrier. Specifically, this study employed the rules methodology that has been developed to be applicable to any kind of oil tankers and bulk carriers, and the direct stress assessment enabling to evaluate the structure response of a specific ship to directly computed stillwater and wave loads.

This study showed that the stillwater loads as expressed in the rules can deviate significantly from the real values reported in the loading manual, especially for the normal ballast conditions for which the rules stillwater bending moment is approximately twice larger than the real value. The rules wave loads were also different from the direct hydrodynamic predictions, especially for head and following seas vertical bending moment amidship for which the direct evaluations are approximately 30% larger than the rules value. Those loads uncertainties can lead to significant deviations in fatigue evaluations.

In order to assess the influence of those various loads uncertainites on the fatigue evaluation, this study assessed the fatigue stress range by three approaches. First, the fatigue stress range was calculated accordingly to the rules loads. Then, using the hot spot stress RAO obtained by the direct stress assessment, spectral analyses were performed to evaluate the reference fatigue stress. Finally, the fatigue stress response to the rules dominant loads was extracted using the equivalent design wave method conducted on the stress RAO. This study compared the fatigue predictions by the three approaches. The following observations can be made:

1. The stillwater loads uncertainties have an effect on the mean stress evaluation. The mean stress can affect the fatigue predictions through the factor for mean stress effect applied on the hot spot stress range, especially regarding the sign of the mean stress. A compressive mean stress can lead to a reduction of the hot spot stress comprised between 80% and 30%, whereas a tension stress can reduce the hot spot stress until 20% only. Furthermore, the total influence is also related to the fraction of life time in which the loading condition led to compressive mean stress which corresponds to approximately half of the ship design life. As a result, this study showed that the stillwater loads uncertainties had a limited effect on the fatigue life prediction.
2. The wave dominant loads uncertainties can have a significant influence on the fatigue evaluation. This

study showed that for the head and following sea load cases, the direct evaluation of vertical bending moment was approximately 30% higher than the rules values. The inaccuracy of the computations performed for this study, especially regarding the hydrodynamic analyses, can partly explain those deviations. Because the hydrodynamic software here employed is of the same kind as those used by the IACS for the rules development, the deviations are thus supposed to be mostly due to the ability of the IACS to calibrate the results on full-scale measurements. The loads uncertainties effect on the hot spot stress assessment was more significant for structural members that are not subjected to additional loads (i.e. sea/ballast/cargo pressure) such as the deck members examined in this study.

3. For the structural members subjected to additional loads, the level of hot spot stress range evaluated by the direct spectral analysis was lower than expected in view of the wave loads assessed by the rules and by direct computations. Therefore, this study compared the hot spot stress range evaluated by the EDW methods to the rules value, and showed that the subjected load reduced the hot spot stress obtained for the same dominant rules loads values. It can thus be concluded that the subjected loads would be underestimated in the rules.

Finally, the fatigue life predictions obtained by direct spectral analyses deviated significantly from the rules evaluations. Therefore this study confirmed that the rules stillwater and wave loads uncertainties can largely affect the fatigue prediction. Besides, the EDW approach presented in this study produced significantly higher fatigue life predictions compare to the rules whereas the dominant load were identical to the rules values. However, this approach does not correspond to the rules methodology. Further investigations should thus be made before validating this approach.

REFERENCES

[1] IACS, 2014. *Harmonized Common Structural Rules for Bulk Carriers and Oil Tankers*. IACS, London.

[2] IMO, 2010. *Adoption of the international goal-based ship construction standard for Bulk Carriers and Oil Tankers*. MSC.290(87), Maritime Safety Committee (MSC).

[3] IACS, 2014. 'Uncertainties Related to the Fatigue Assessment Procedure'. *Technical Background Report for the CSR-H*, IACS, London.

[4] Maddox, S.J., 2001. 'Recommended design S-N curve for fatigue assessment of FPSOs'. 11th ISOPE, Stavanger.

[5] Fricke, W., 2001. 'Recommended hot spot analysis procedure for structural details of FPSOs and ships on round robin FE analysis'. 11th ISOPE, Stavanger.

[6] Lotsberg, I., 2006. 'Fatigue design of plated structures using finite element analysis'. *Journal of ship and offshore structures*, Vol. 1, pp. 45-54.

[7] Lotsberg, I., Rundhaug, T.A., Thorkildsen, H., Bøe, A., and Lindemark, T., 2008. 'A procedure for fatigue design of web-stiffened cruciform connections'. SAOS, Vol. 3, pp. 113-126.

[8] Parunov, J., Corak, M., and Gilja, I., 2013. 'Calculated and prescribed stress concentration factors of ship side longitudinal connections'. *Engineering Structures*, Vol.52, pp.629–641.

[9] IACS, 2014. 'Hull Girder Vibration', *Technical Background Report for the CSR-H*, IACS, London.

[10] Hirdaris, S.E., Bai, W., Dessi, D., Ergin, A., Gue, X., Hermundstad, O.A., Huijsmans, R., Iijima, K., Nielsen, U.D., Parunov, J., Fonseca, N., Papanikolaou, A., Argyriadism, K., and Incecik, A., 2014. 'Loads for use in the design of ships and offshore structures'. *Ocean Engineering*, Vol.78, pp. 131-174.

[11] Guedes Soares, C., and Moan, T., 1991. 'Model Uncertainty in the Long-term Distribution of Wave-induced Bending Moments For Fatigue Design of Ship Structures'. *Marine Structures*, Vol.4, pp. 295-315.

[12] Bitner-Gregersen, E.M., Cramer, E.H., and, Løseth, R., 1995. 'Uncertainties of Load Characteristics and Fatigue Damage of Ship Structures'. *Marine Structures*, Vol.8, pp. 97-117.

[13] British Marine Technology (Primary contributors Hogben N., Da Cunha, L.F. and Oliver, H.N.), 1986. *Global Wave Statistics*, Unwin Brothers Limited, London.

[14] Bitner-Gregersen, E.M., Cramer, E.H., and Korbijin, F., 'Environmental Description for Long-term Load Response of Ship Structures', ISOPE June 1995, The Hague, The Netherlands.

[15] IACS, 2001. 'Standard Wave Data'. *Recommendation (Rec.) No.34*, IACS, London.

[16] Derbanne, Q., Rezende, F., de Hauteclocque G., and Chen, X.B., 2011. 'Evaluation of Rule-Based Fatigue Design Loads Associated at a New Probability Level', 21st ISOPE, Hawaii, USA.

[17] IACS, 2014. 'Equivalent Design Wave (EDW) for Fatigue Loads'. *Technical Background Report for the CSR-H*, IACS, London.

[18] Parunov, J., Senjanović, I., and Pavićević, M., 2004. 'Use of Vertical Wave Bending Moments From Hydrodynamic Analysis In Design of Oil Tankers'. *International Journal of Maritime Engineering*, (Transactions RINA Part A4), Vol.146, pp 51-64, 2004.

[19] IACS, 2010. 'Longitudinal Strength Standard'. *Unified Requirement (UR) S11*, IACS, London.

[20] Quéméner, Y., Chen, K.C., Lee, C.F. and Huang, C.H., 2014. 'Fatigue life evaluation of an oil tanker employing direct hydro-structure computations - A comparison with the CSR-H approach'. International Conference on Safety & Reliability of Ships, Offshore & Subsea Structures, Glasgow, UK.

[21] Malenica, S., Sireta, F.X., Bigot, F., Wang, C., and Chen, X.B., 2009. 'Some aspects of hydro-structure coupling for combined action of seakeeping and sloshing'. 28th OMAE, Honolulu, USA.